JAERI-M
87-011

SOFT X-RAY MEASUREMENTS OF THE JT-60 TOKAMAK PLASMA IN THE INITIAL EXPERIMENTS

February 1987

Takeo NISHITANI, Keisuke NAGASHIMA
and Hiroshi TAKEUCHI

日本原子力研究所
Japan Atomic Energy Research Institute

JAERI-Mレポートは，日本原子力研究所が不定期に公刊している研究報告書です。
入手の問合わせは，日本原子力研究所技術情報部情報資料課（〒319-11茨城県那珂郡東海村）あて，お申しこしください。なお，このほかに財団法人原子力弘済会資料センター（〒319-11茨城県那珂郡東海村日本原子力研究所内）で複写による実費頒布をおこなっております。

JAERI-M reports are issued irregularly.
Inquiries about availability of the reports should be addressed to Information Division Department of Technical Information, Japan Atomic Energy Research Institute, Tokai-mura, Naka-gun, Ibaraki-ken 319-11, Japan.

編集兼発行　日本原子力研究所
印　　刷　㈱高野高速印刷

JAERI-M 87-011

Soft X-ray Measurements of the JT-60 Tokamak Plasma in the Initial Experiments

Takeo NISHITANI, Keisuke NAGASHIMA and Hiroshi TAKEUCHI

Department of Large Tokamak Research
Naka Fusion Research Establishment
Japan Atomic Energy Research Institute
Naka-machi, Naka-gun, Ibaraki-ken

(Received January 26, 1987)

The X-ray pulse height analysis in the energy range of 3-60 keV was performed for JT-60 ohmically heated and initial neutral beam heated plasma, using a liquid-nitrogen cooled high purity germanium detector. The time evolution of the electron temperature was derived from the measured spectra with the time resolution of 100 ms. The electron temperature was obtained up to 3.0 keV in the typical divertor ohmically heated discharges with plasma current 2 MA. The dominant metal impurity is titanium. The typical impurity density and the effective ionic charge Z_{eff} were estimated from these measurements, and the titanium density of 10^{-3} % and Z_{eff} of 1.2 were could be obtained for the typical ohmically heated divertor discharges. And the titanium densities of neutral beam heating discharges are about factor 2 larger than ones of ohmically heating.

Keywords: Soft X-ray, JT-60, Pulse Height Analysis, High Purity Germanium Detector, Electron Temperature, Tokamak Plasma

ＪＴ－60トカマクプラズマ初期実験における軟Ｘ線測定

日本原子力研究所那珂研究所臨界プラズマ研究部
西谷健夫・永島圭介・竹内　浩

（１９８７年１月２６日受理）

ＪＴ－60のジュール実験及び初期中性粒子入射加熱実験において，液体窒素冷却した高純度ゲルマニウム検出器を用いて軟Ｘ線の波高分析測定を実施した。１００ｍｓの時間分解能で軟Ｘ線スペクトルを測定することにより，電子温度の時間変化が測定された。得られた電子温度はプラズマ電流2MAのダイバータジュール加熱放電において3.0keV程度まで達した。また，得られた軟Ｘ線スペクトルより，主な金属不純物はチタンであった。ジュールプラズマにおける典型的なチタン密度は平均電子密度の10^{-3}％程度であり，この時の実効電荷数は約1.2と推定された。さらに，中性粒子入射加熱時のチタン密度はジュール加熱時の概ね２倍程度であった。

那珂研究所：〒311－02　茨城県那珂郡那珂町大字向山801－1

Contents

I. Introduction 1
II. Experimental set-up 2
III. Analysis of soft X-ray spectrum 5
IV. Results 9
A. Electron temperature 9
B. Impurity concentration 10
V. Discussion and conclusion 12
Acknowledgement 12
Reference 13

目　　次

I　序 1
II　実験装置 2
III　軟X線スペクトラムの分析 5
IV　結果 9
A　電子温度 9
B　不純物密度 10
V　結果と考察 12
謝辞 12
参考文献 13

I. INTRODUCTION

One of the main objectives of JT-60 tokamak is to study the impurity behavior in a near-reactor size machine, of which plasma minor radius is 0.95 m and major radius is 3.0 m. In order to estimate the electron temperature and to investigate the basic performance of impurities in JT-60, the X-ray pulse height analyzer (PHA)[1] was constructed. The high purity germanium detector cooled by liquid-nitrogen is used to measure the soft X-ray spectra in the 3-60 keV energy range with time resolution of 100 ms. The X-ray spectrum consists of an exponentially decreasing continuum spectrum, due to bremsstrahlung and recombination radiation, and line radiation of high Z impurities. Electron temperature can be derived from the inclination of the continuum spectrum, and the concentrations of low- and high-Z impurities can be derived from the absolute measurements of the continuum and line radiation.

The experimental set-up of the PHA system is described in detail in Sec. II. The analysis procedure of soft X-ray spectrum is reviewed in Sec. III. In the last section the experimental results for measurements of electron temperature and the impurity concentrations are presented.

II. EXPERIMENTAL SET-UP

The spatial arrangement of the pulse-height analyzer on the JT-60 is shown in Fig. 1. The pulse-height analyzer is installed on the basic structure at P-18 port section and views the center of the plasma through the vertical port. The detailed view of the pulse-height analyzer system is shown in Fig. 2. It is connected to the vacuum vessel of the JT-60 by about 4 m long inconel tube and the pumping system using a turbo molecular pump.

The high purity germanium detector arranged at the bottom of this system is cooled by liquid nitrogen using the J-shaped cold finger. The high purity germanium crystal is mounted behind 0.025 mm thick beryllium window which keeps it vacuum which is isolated from the vacuum environment of JT-60. The crystal has an active area of about 80 mm^2 and most sensitive between 2 and 100 keV. The efficiency of the detector is 80% for 5.9 keV photon, which is caliblated by ^{55}Fe X-ray source. As the photon of which energy is greater than 100 keV penetrates the crystal which is 10 mm thick, the efficiency is reduced. An energy resolution of the detector, using a 1-μs amplifier time constant, is 390 eV FWHM for 5.9 keV photons.

The detector views the plasma through the collimator and the thin-foil filter placed in front of the detector. The collimator is made of the 5mm-thick lead disk covered by 5mm aluminium side by side, on which eight different diameter apertures are arranged coaxially. The X-ray intensity incident on the detector is remotely controlled by this rotating collimator disk. The apertures provide a large dynamic range of 10^3 in count rate to adjust the various conditions of JT-60 plasma. The Jeneva gias system is employed for the transmission between the collimator disk and the moter in order to set the center of the aperture to the detector axis precisely. A set of filters, which consists of 4 beryllium foils and 4 aluminium foils displaced on the aluminium disk, can be remotely set to adjust the cut off energy of the incident photons. The driving mechanism of the filter disk is same as one of the collimator disk. Too many photons incident on the detector increase the probability of pulse pile up. Fig. 3 shows normal and pile up spectra of soft X-ray measured on the JT-60. The pulse pile up becomes remarkable at more than 40 KHz count rate for

this detection system. Therefore, the count rate has to be kept 10-40 KHz by choosing the suitable aperture and foil.

Ceramic breaks in front of the gate valve isolate the supporting structure of the pulse height analyzer from the differential pumping system and the vacuum vessel electrically. Furthermore, the detector is isolated from the supporting structure by a poli-ether-ether-keton break which is able to use instead of a conflat type gasket and to be baked up to 180 ^{o}C. The 30mm-thick iron cylinder surrounds the detector and the pre-amplifier, which are prevented against the influence of the leakage magnetic field from the JT-60 and the electro-magnetic noise. Lead plates on the iron cylinder shield hard X-rays which are generated by runaway electrons collided with the limiters.

The block diagram of the electronics is shown in Fig. 4. Charges generated by a X-ray photon in the detector are integrated by the charge sensitive pre-amplifier. The time constant of the pre-amplifier is made as short as possible in order to get higher count rate. The gain of the linear amplifier is adjusted so high for the initial experiments of the JT-60 that the energy range of measurement is from 3 to 60 keV. Though the amplifier has the pile up rejection circuit, it was not used in this experiment. Because the gain is set high in this experiment, the pile-up rejector is triggered by the thermal noise and then generates the event pulses of pulse pile up continuously. Shorter shaping time constant makes count rate higher, however, degrades an energy resolution. So the time constant of the amplifier is set 1-μ sec.

At the time of 1-minute before shot, shot-start and shot-end, 8-bit corded timing signals are sent to the timing reciever (TGR) via fiber optics from Zenkei which is the computer system for JT-60 facility control. When the TGR gets the timing signal of shot-start, it distributs the start trigger to the timing generater (TMG). Then the TMG generates the sampling clocks for the ADC and the scaler, of which the frequencies are determined individually by the program coded in the auxiliary crate controller (ACM). The conversion gain of the ADC is able to be adjusted among 256, 512 and 1024 by the program of ACM. The degitized data by the ADC is transferred to four 32 KW histogram memories via the data router. Then, for example, a histgram

of 1024 channels can be stored at each time interval of 100m sec throughout 12.8 sec. The scaler records the total count rate of the pulses above a discrimination level which is same as that of the ADC. Furthermore, the dead time of the PHA system is estimated from the difference between the count rate of the scaler and that of the ADC.

Data acquisition system has a hierarchical structure consisting of the ACMs and the inter shot processer (ISP) which is a general purpose large computer. The ACM with a i8086 processer controls the PHA system via 5M Byte/s optical CAMAC serial highway. Following a plasma shot, the ACM sends the measurement parameters, for example, a diameter of the collimator, material and thickness of the foil, sampling time, etc, via a similar serial highway. The data from the ADC and the scaler are collected by the ISP via 2 level serial highways directly. Then the processing in ISP corrects the filter attenuation, the detector efficiency and solid angle for the raw data and, further more during a inter-shot, makes the calculation of the electron temperature and the impurity analysis. When the ACM is isolated from the ISP, the ACM can independently calculate and display the time evolution of electron temperature.

III. ANALYSIS OF SOFT X-RAY SPECTRUM

The spectral distribution of the soft X-ray emission in tokamak discharges can yield the valuable information on the electron temperature, impurity concentrations and the presence of runaway electrons. The electron temperature is obtained from the slope of soft x-ray spectrum in a semilogarismic plot, but the interpretation is complicated by radial profile effect, because the measured spectra are the line integral signals. The absolute intensity of the continuum radiation compared to only hydrogen bremsstrahlung is represented by the enhancement factor ζ, which characterizes the impurity concentrations in a plasma, as well as the effective ionic charge Z_{eff}. Typical soft X-ray spectrum consists of a continuum spectrum with a few impurity K- and L-lines. If the runaway electrons are produced substantially in the discharges, the high energy runaway tails become prevalent in the continuum spectrum. The metallic impurity concentrations can be estimated from the K- or L-lines spectra, and the residual light impurity concentrations from the enhancement factor ζ.

The X-ray emission from a plasma consists of a continuum of free-free bremsstrahlung and free-bound recombination radiation, and of a bound-bound line radiation. The energy spectrum of bremsstrahlung radiation for a Maxwellian plasma is[2)]

$$\frac{dP_{ff,ij}(T_e,E_\nu)}{dE_\nu} = 3\times10^{-15}\, n_e n_i \frac{n_{ij}}{n_i} Z_{ff,ij}^2 T_e^{-1/2} \bar{g}_{ff,ij} \exp\left(-\frac{E_\nu}{T_e}\right) \quad (1)$$

$$[\mathrm{keV/keV\cdot cm^3\cdot sec}]$$

where i, j represent an i-impurity ion species and j-charge state. E_ν, n_e, T_e represent the photon energy, electron density and electron temperature, respectively. $Z_{ff,ij}$ is the effective ionic charge for free-free bremsstrahlung, which is nearly equal to the nuclear charge[3)]. $\bar{g}_{ff,ij}$ is the averaged free-free gaunt factor which is averaged over a Maxwellian electron velocity distribution, and is a function depending on the electron temperature and photon energy. n_i

is the total density of the i-impurity species, and n_{ij}/n_i is the relative density ratio of the j-ionic charge state of the impurity.

The formula of free-bound radiative recombination,[2] which is obtained from the Kramers formula for the hydrogenic ions, is

$$\frac{dP_{fb,ij}(T_e,E_\nu)}{dE_\nu} = 3\times10^{-15}\, n_e n_i \frac{n_{ij}}{n_i} Z_{ij}^2\, T_e^{-1/2}\, \beta_{ij}\, \mathrm{Exp}(-\frac{E_\nu}{T_e}) \qquad (2)$$

$$\beta_{ij}(T_e,E_\nu) = \frac{\xi}{n^3}\,\bar{g}_{fb,ij}\,\frac{I_{ij}}{T_e}\exp(\frac{I_{ij}}{T_e})\,\theta\,(E_\nu - I_{ij})$$

$$+ \sum_{\alpha=1}^{\infty}\frac{2}{(n+\alpha)}\,\bar{g}_{fb,ij}\,\frac{Z_{ij}^2\cdot I_H}{(n+\alpha)^2 T_e}\exp\left(\frac{Z_{ij}^2\cdot I_H}{(n+\alpha)^2 T_e}\right)\theta\,(E_\nu - I_{ij,n+\alpha})$$

where Z_{ij} is the charge of ij-ion before recombination and I_H and I_{ij} are the ionization potentials of hydrogen and the recombined electron in a ground state, respectively. The first term in β_{ij} represents the recombination to the valence shell-n with empty spaces ξ and the second term is the contribution to the quantum states $(n+\alpha)$. As the photon energy is the sum of the kinetic and binding energies of the recombining electron, the spectrum has the recombination steps at the energies equal to $I_{ij,n+\alpha}$, and is indicated by the step function $\theta(E_\nu - I_{ij,n+\alpha})$. $\bar{g}_{fb}$ is the averaged free-bound gaunt factor and assumed to be unity in most cases[8].

From Eqs.(1) and (2), total X-ray spectrum is given using the enhancement factor ζ.

$$\frac{dP_{tot}(T_e,E_\nu)}{dE_\nu} = \sum_i\sum_j\left\{\frac{dP_{ff,ij}}{dE_\nu} + \frac{dP_{fb,ij}}{dE_\nu}\right\}$$

$$= 3\times10^{-15}\,\zeta\cdot\bar{g}_{ff,H}\, n_e^2\, T_e^{-1/2}\exp(-\frac{E_\nu}{T_e}) \qquad (3)$$

Here we define the factor γ_{ij} as well as in ref.(3), and the relation between γ_{ij} and ζ is given as

$$\frac{dP_{tot,ij}}{dE_\nu} = \gamma_{ij}\,\frac{dP_{ff,ij}}{dE_\nu} \qquad (4)$$

$$\gamma_{ij} = \frac{\beta_{ij} \cdot Z_{ij}^2}{\bar{g}_{ff,ij} \cdot Z_{N,i}^2} + 1 \tag{5}$$

$$\gamma_i = \sum_j \gamma_{ij} \frac{n_{ij}}{n_i} \tag{6}$$

$$\zeta = \frac{1}{\bar{g}_{ff,H}} \sum_i \frac{n_i}{n_e} \gamma_i \bar{g}_{ff,i} Z_{N,i}^2 \tag{7}$$

The charge state fractions of an i-ion are unknown, which is dominated by the balance between ionization and recombination and in considerably affected by the radial direction particle transport. But for the light impurities, it can be assumed that all ions are stripped pertectly.

The dominant processes of the bound-bound line radiation are thought to be electron collisional excitation and dielectronic recombination[6]. For metallic impurities, K- or L-line photons are emitted in the energy range where the PHA detectors are sensitive, which characterize the impurity elements and their concentrations. The photon emissivity of i-ion S_i[photons/cm^3·sec] is represented by

$$S_i = n_e n_i \sum_j \frac{n_{ij}}{n_i} \langle \sigma v \rangle_{ij} \tag{8}$$

where $\langle \sigma v \rangle_{ij}$ is the total excitation rate averaged over a Maxwellian velocity distribution[6),7)]. The line integrated value is

$$S_L = \left(\frac{\overline{n_i}}{n_e} \right) \int n_e(r)^2 \langle \sigma v \rangle_i \, d\ell \tag{9}$$

where $\sum_j (n_{ij}/n_i) \langle \sigma v \rangle_{ij} = \langle \sigma v \rangle_i$ and $(\overline{n_i/n_e})$ is the averaged impurity density for the X-ray emitting high temperature region. This value is related to the detected photon count rate C [count/sec] as

$$C = \varepsilon_f \varepsilon_d S_d \frac{\Delta\Omega}{4\pi} S_L \tag{10}$$

where ε_f, ε_d, S_d, $\Delta\Omega/4\pi$ represent the filter transparency, detector efficiency, detector sensitive area and solid angle, respectively.

The neutrality of plasma is represented by

$$n_e = n_p + \sum_{i \neq p} Z_i \, n_i \tag{11}$$

where n_p is proton density. Therefore the effective ionic charge Z_{eff} is given by

$$Z_{eff} = \frac{\sum_{i \neq p} (Z_i^2 - Z_i) n_i}{n_e} \tag{12}$$

IV. RESULTS

Fig. 5 shows the typical spectrum of the soft X-ray emitted from the main plasma in JT-60 divertor discharge. In the spectrum, K_α and K_β lines of titanium and K_α of nickel are identified. The former is the coating material of the first wall and the latter is the base metal of inconel 625, of which the JT-60 first wall is made. No significant lines of molibdenum, which is the base material of the limiter, were observed in the normal discharges. In the following sections, we briefly describe the electron temperature and the impurity concentration from the soft X-ray PHA measurements.

A. ELECTRON TEMPERATURE

Fig. 6 shows the time evolution of the plasma current, electron density and electron temperature from PHA for the divertor discharge of I_p=1.5MA, B_T=4.5T. The electron density is increasing gradually and reaches its peak at about 7.0 sec, when inversely the electron temperature shows minimum value. This tendency is more remarkable in Fig. 7. This data is obtained from the plasma current flat top phases. As the electron density increases, the effective ionic charge decreases. So the ohmic input power decreases and therefore the electron temperature decreases.

The pulse height analyzer measures the line integrated spectrum along the viewing chord and it represents the central high temperature region. The profile effect is approximately less than 10% in the central electron temperature. In Fig. 8 the temperature obtained by PHA analysis is compared with the central electron temperature measured by Thomson scattering. In this figure, PHA temperature is a little higher than Thomson scattering temperature. But the good agreement is obtained in the statistical error range.

B. IMPURITY CONCENTRATION

In JT-60 plasma, the dominant metal impurity species are titanium, nickel and chromium. In Fig. 5 these impurity lines are seen except chromium line, of which K_α-line is overlapped on Ti-K_β line. During the strong neutral beam heating discharges, the Mo-K_α line which is generated on the divertor plate has been observed and these discharges were often terminated by the hard radiation energy loss.

Fig. 9 shows the effective ionic charge Z_{eff} as the function of electron density. As the electron density increases, Z_{eff} approaches asymptotically the value of 1. The dependence of Z_{eff} on the plasma current is not clear, but the values of limiter discharges are far larger than ones of divertor discharges. No difference between the ohmic and neutral beam heating discharges can be seen and this result is supported by the visible bremsstrahlung spectroscopy. The value of Z_{eff} estimated by PHA is 1.2 at $\bar{n}_e = 3.0\times10^{13}$ cm^{-3}, but the values obtained by the other diagnostics, the visible bremsstrahlung spectroscopy and the active beam scattering system, are about 1.5 at the same electron density. This deviation is under examination. In order to calculate Z_{eff}, titanium and nickel are included as the dominant metal impurities and oxygen is assumed to be only light impurity because of the lack of enough spectroscopic information. The electron density and temperature profile are given from the 4ch interferometers and 6ch Thomson scattering measurements, respectively.

In Fig. 10, the titanium concentrations of the divertor and limiter discharges which are estimated from Ti-K_α photons are shown as the function of electron density. The symbol of He shows the helium discharges and all the others are hydrogen discharges. To calculate the excitation rate coefficient, the dominant three processes are considered; the electron collisional excitation[6),7)], the dielectronic recombination and the radiative recombination into the K-shell. The titanium concentrations of neutral beam heating discharges are about factor 2 larger than ones of ohmically heating. The values of helium discharges are far larger than ones of hydrogen dishcarges, but the exponentially decreasing features with the increasing of electron density can be seen in all discharges.

Fig. 11 shows oxygen concentration as the function of electron density. It decreases with the increasing of electron density as well as titanium concentration, but its decline is smaller than one of titanium. The oxygen concentrations of limiter discharges are about factor 5 larger than ones of divertor discharges, but no clear defference can be seen between ohmic and neutral beam heating discharges for the divertor discharges. These values estimated by PHA are about factor 2 smaller than ones obtained by the active beam scattering system.

V. DISCUSSION AND CONCLUSION

The X-ray pulse height analysis was performed using a liquid-nitrogen cooled high purity germainum detector and by this measurement the electron temperature and impurity concentrations could be estimated. The electron temperature measured by PHA, which is not the central electron temperature strictly but represents the central high temperature region, corresponds to the temperature measured by Thomson scattening system within the statistical error range. The titanium concentration is decreasing exponentially with the increasing of electron density and its typical value is 1.0×10^{-3}% at $\bar{n}_e=3.0\times10^{13}$ cm^{-3}. About the effective ionic charge Z_{eff} which is dominated by light impurities in JT-60 plasma, there is the unnegligible difference between the PHA measurement and others; the visible bremsstrahlung spectroscopy and the active beam scattering system. This difference may be due to the ambiguity of the atomic cross section considered in the calculation process or due to the system calibration error.

Acknowledgement

The authors wish to thank the members of the JT-60 team for their efforts and Drs. M. Shiho, H. Maeda and Y. Suzuki for their helpful advice. We would like to express our gratitude to Drs. S. Tamura and M. Yoshikawa for their continuous encouragement to the present work.

V. DISCUSSION AND CONCLUSION

The X-ray pulse height analysis was performed using a liquid-nitrogen cooled high purity germainum detector and by this measurement the electron temperature and impurity concentrations could be estimated. The electron temperature measured by PHA, which is not the central electron temperature strictly but represents the central high temperature region, corresponds to the temperature measured by Thomson scattening system within the statistical error range. The titanium concentration is decreasing exponentially with the increasing of electron density and its typical value is 1.0×10^{-3}% at $\bar{n}_e=3.0\times10^{13}$ cm^{-3}. About the effective ionic charge Z_{eff} which is dominated by light impurities in JT-60 plasma, there is the unnegligible difference between the PHA measurement and others; the visible bremsstrahlung spectroscopy and the active beam scattering system. This difference may be due to the ambiguity of the atomic cross section considered in the calculation process or due to the system calibration error.

Acknowledgement

The authors wish to thank the members of the JT-60 team for their efforts and Drs. M. Shiho, H. Maeda and Y. Suzuki for their helpful advice. We would like to express our gratitude to Drs. S. Tamura and M. Yoshikawa for their continuous encouragement to the present work.

REFERENCES

(1) K.W. Hill, M. Bitter, M. Diesso, L. Dudek, S. Von Goeler, S. Hayes, L.C. Johnson, J. Kiraly, E. Moshey, G. Renda, S. Sesnic, N.R. Sauthoff, F. Tenney, and K. M. Young; Rev. Sci. Instrum., Vol.56, No.5, 840(1985).

(2) E.H. Silver, M. Bitter, K. Brau, D. Eames, A. Greenberger, K.W. Hill, D.M. Meade, W. Roney, N.R. Sauthoff, and S. Von Goeler; Rev. Sci. Instrum. Vol.53, No.8, 1198(1982).

(3) S. Von Goeler, W. Stodiek, H. Eubank, H. Fishman, S. Grebenshchikov, E. Hinnov; Nucl. Fusion 15, 301(1975).

(4) K.W. Hill, M. Bitter, N.L. Bretz, M. Diesso, P.C. Efthimion, S. Von Goeler, J. Kiraly, A.T. Ramsey, N.R. Sauthoff, J. Schivell, and S. Sesnic; PPPL-2309 (1986).

(5) K.H. Behringer, P.G. Carolan, B. Denne, G. Decker, W. Engelhardt, M.J. Forrest, R. Gill, N. Gottardi, N.C. Hawkes, E. Kallne, H. Krause, G. Magyar, M. Mansfield, F. Mast, P. Morgan, N.J. Peacock, M.F. Stamp, H.P. Summers; Nucl. Fusion 26, 751 (1986).

(6) C. Breton, C. De Michelis, and M. Mattioli; J. Quant. Spectrosc. Radiat. Transfer 19, 367 (1978).

(7) C. De Michelis, M. Mattioli; Nucl. Fusion 21, 677 (1981).

(8) A. Costescu, N. Mezincescu; Phys. Lett. A 29, 359 (1984).

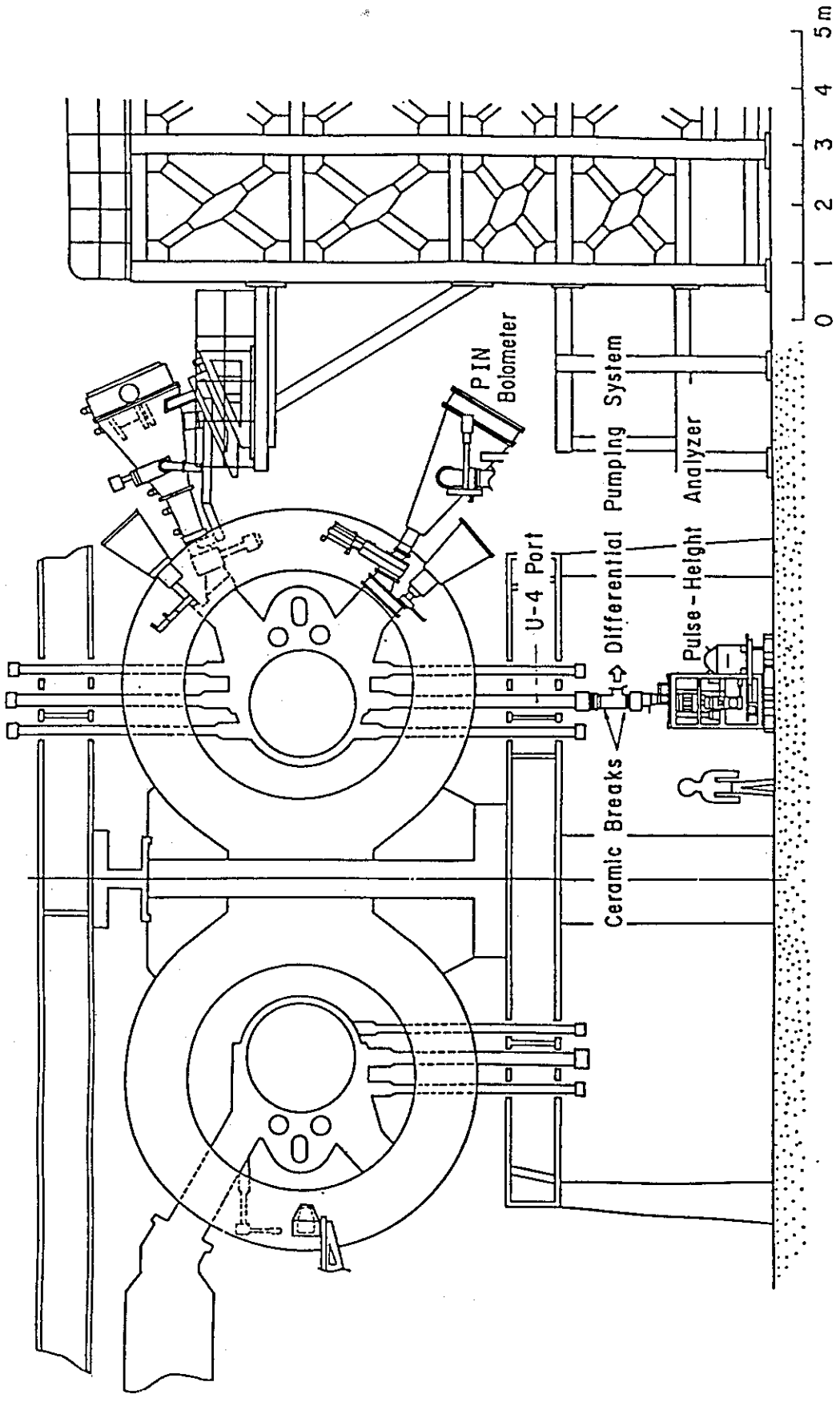

Fig. 1 Spatial arrangement of the pulse height analyzer on JT-60.

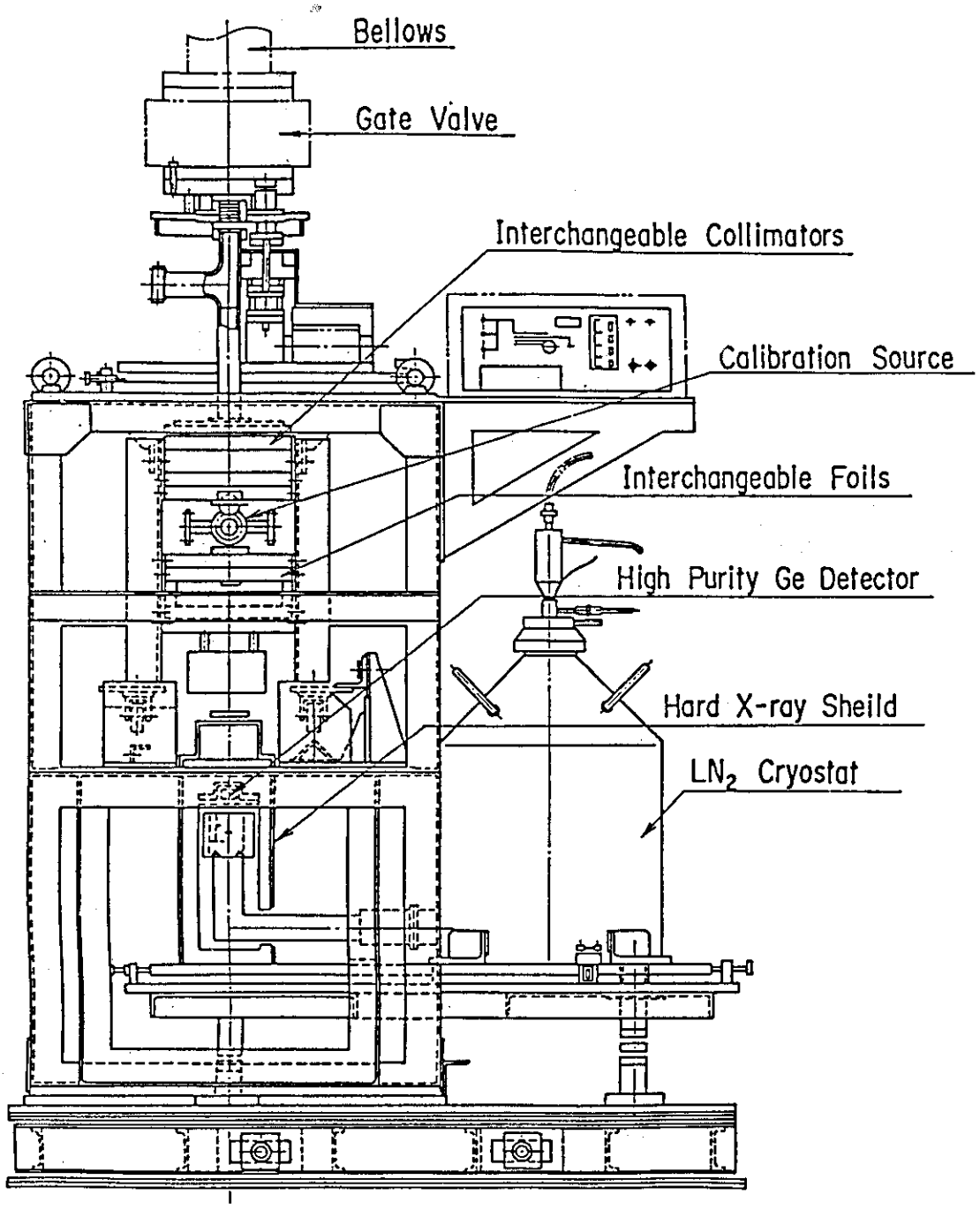

Fig. 2 The detailed constitution of the pulse height analyer.

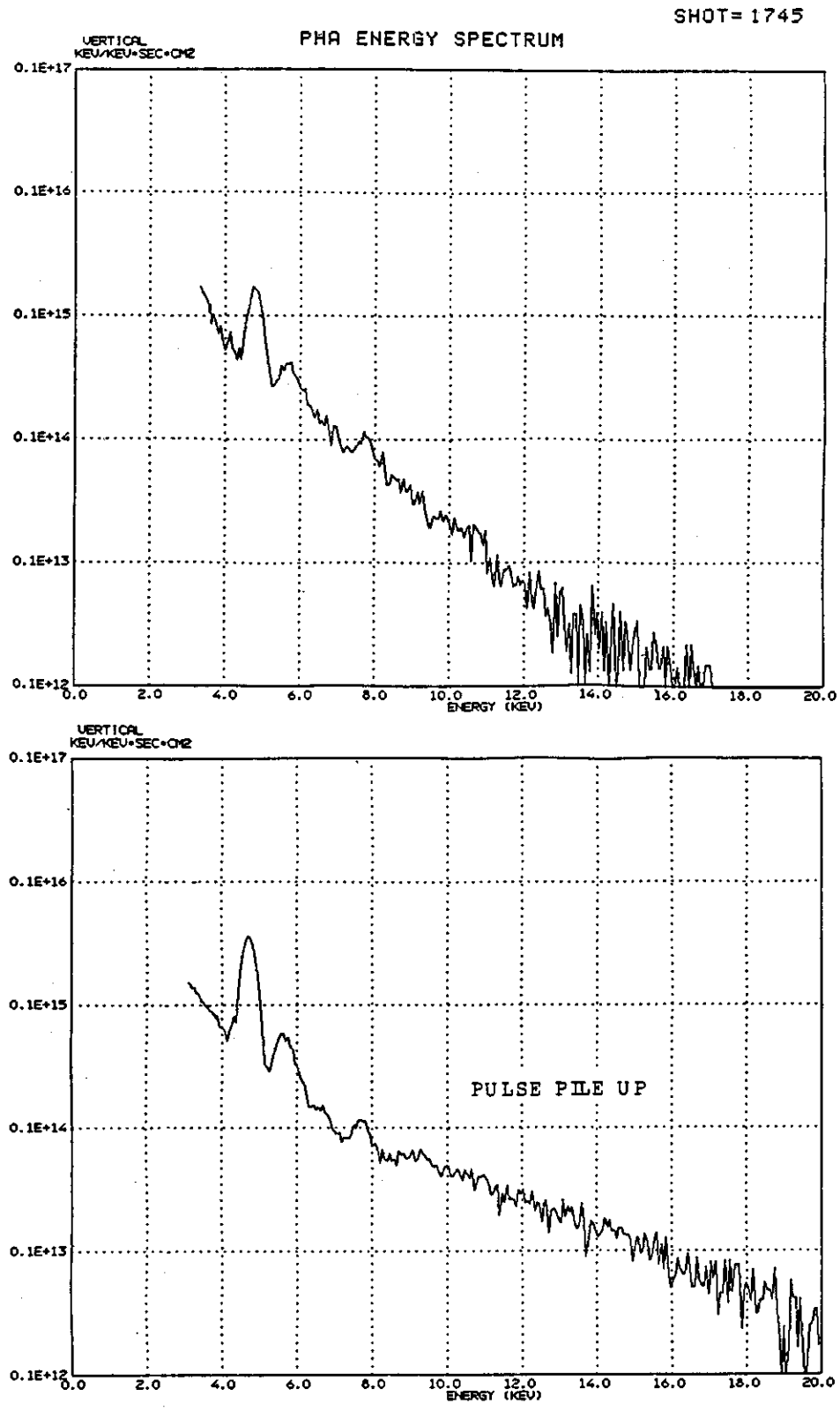

Fig. 3 Typical spectrum with and without pulse pile up.

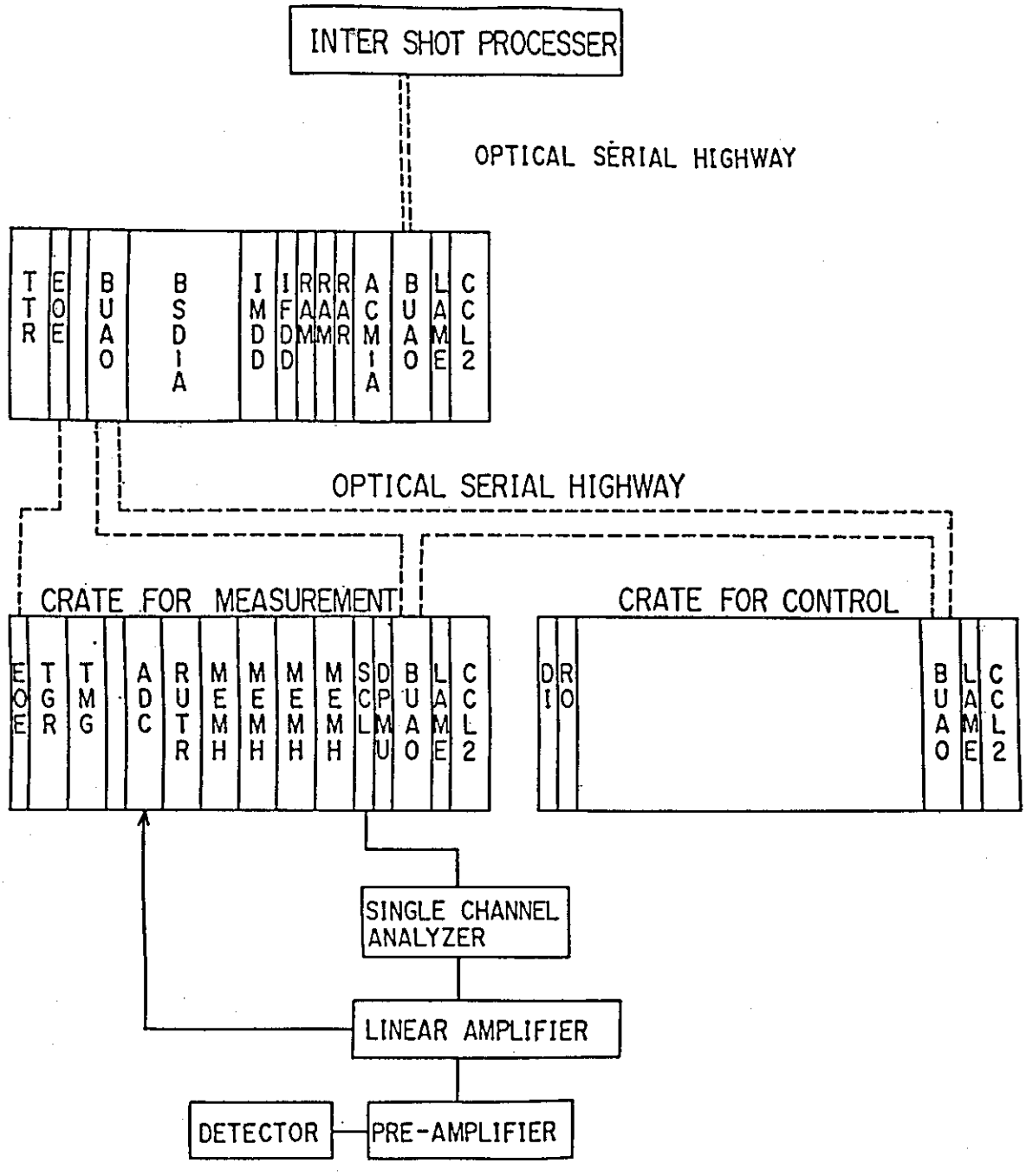

Fig. 4 Block diagram of the electronics in JT-60 pulse height analyzer

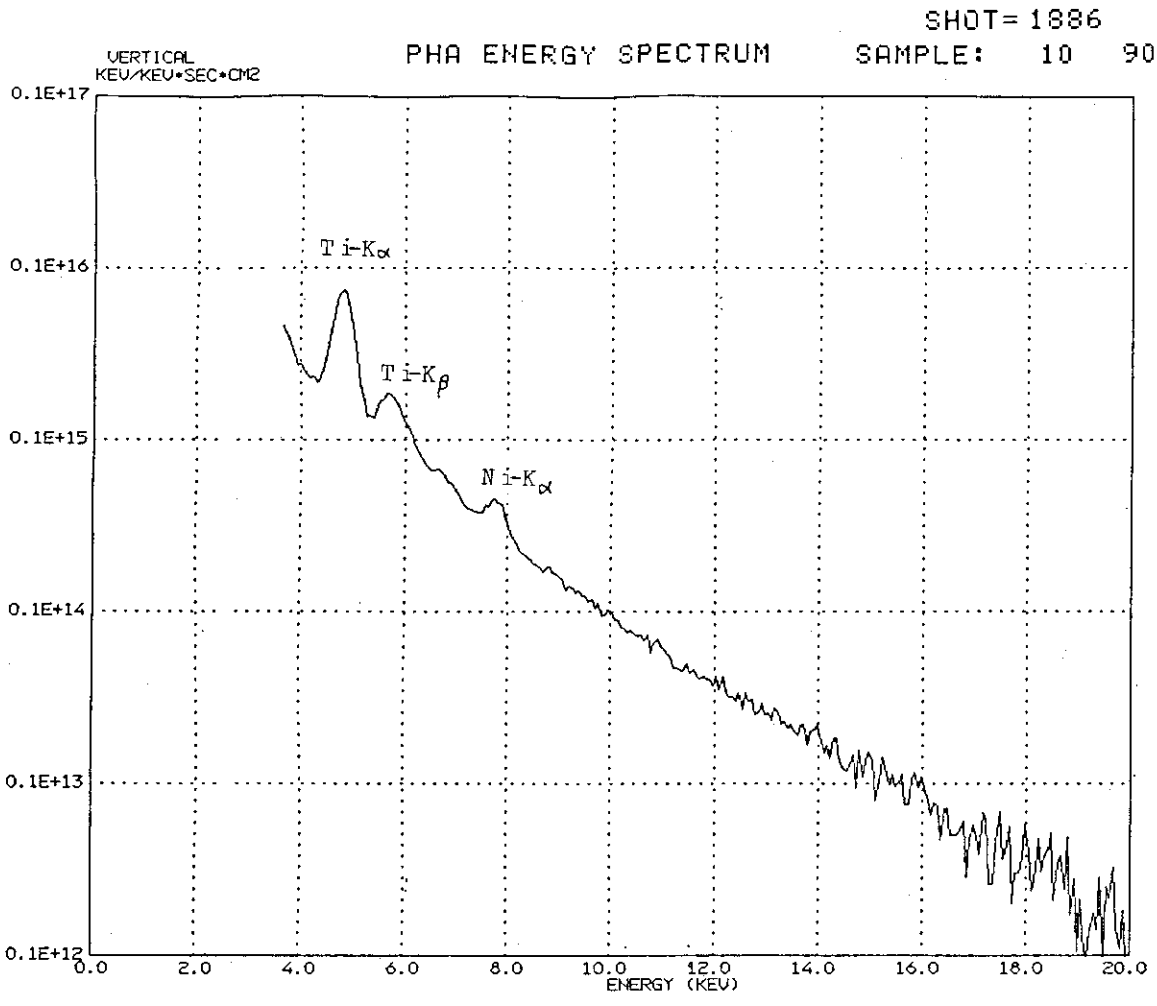

Fig. 5 Typical soft X-ray spectrum of 1.5 MA divertor discharge. Titanium and nickel lines are identified on continuum radiation spectrum.

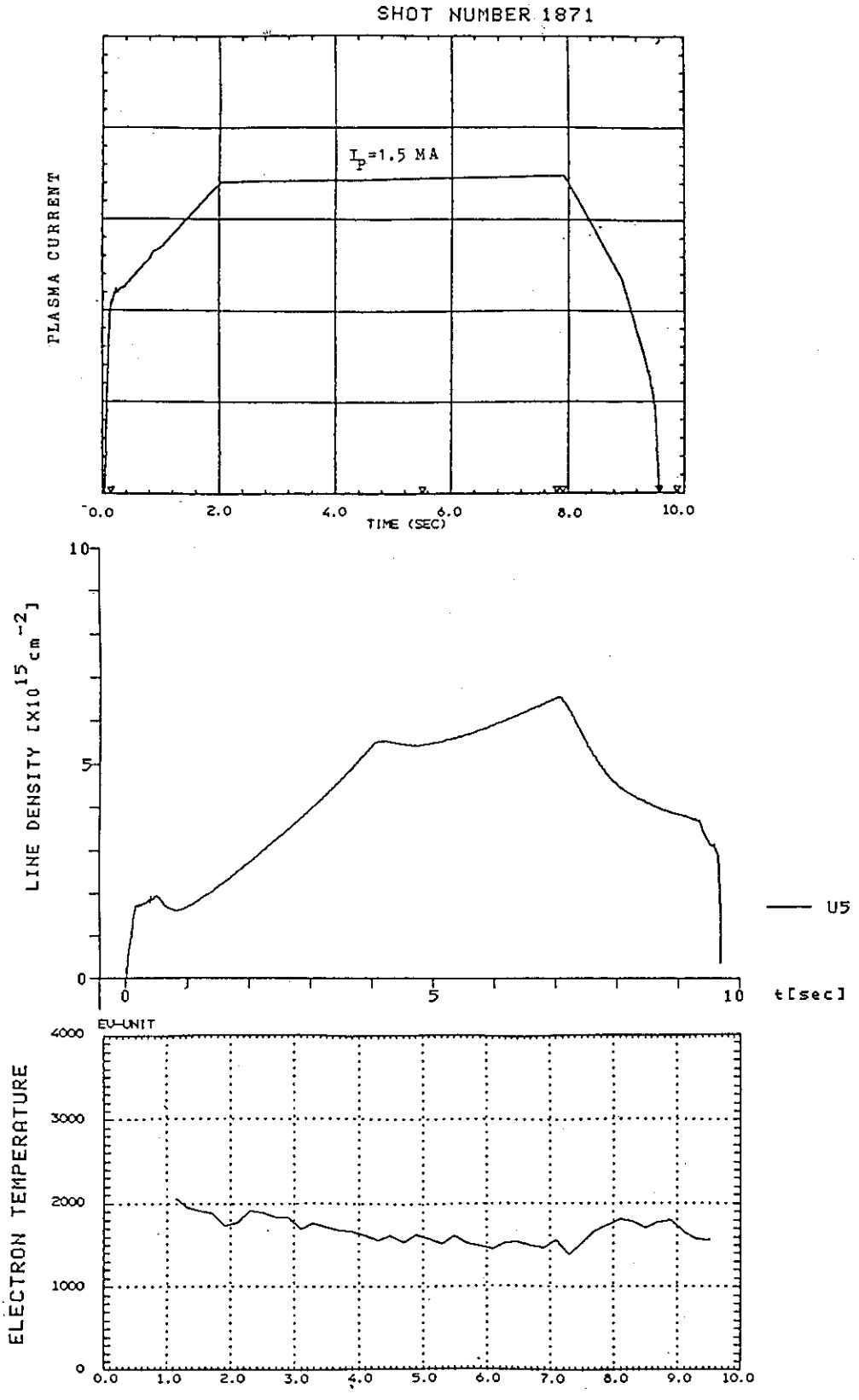

Fig. 6 Time evolution of plasma current, electron density and electron temperature measured by PHA diagnostics.

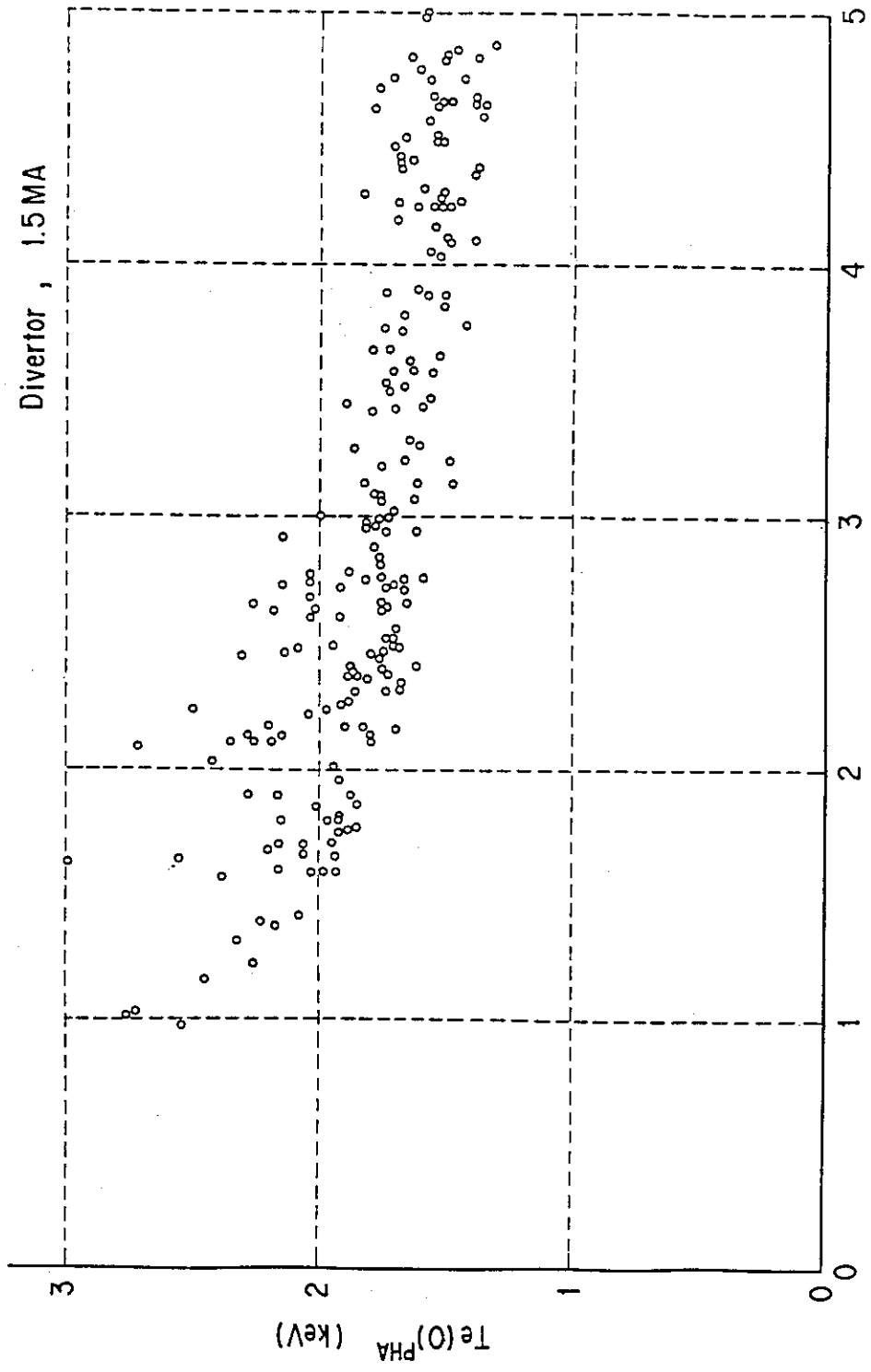

Fig. 7 Electron temperature measured by PHA system as a function of electron density on the condition of I_p=1.5 MA, B_T=4-4.5T.

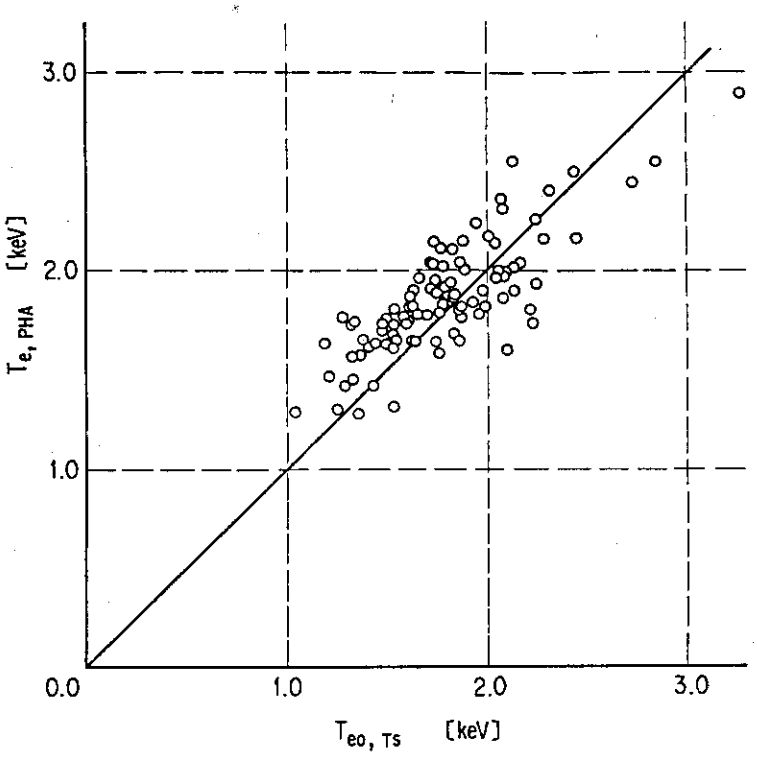

Fig. 8 Electron temperature measured by PHA versus Thomson scattering.

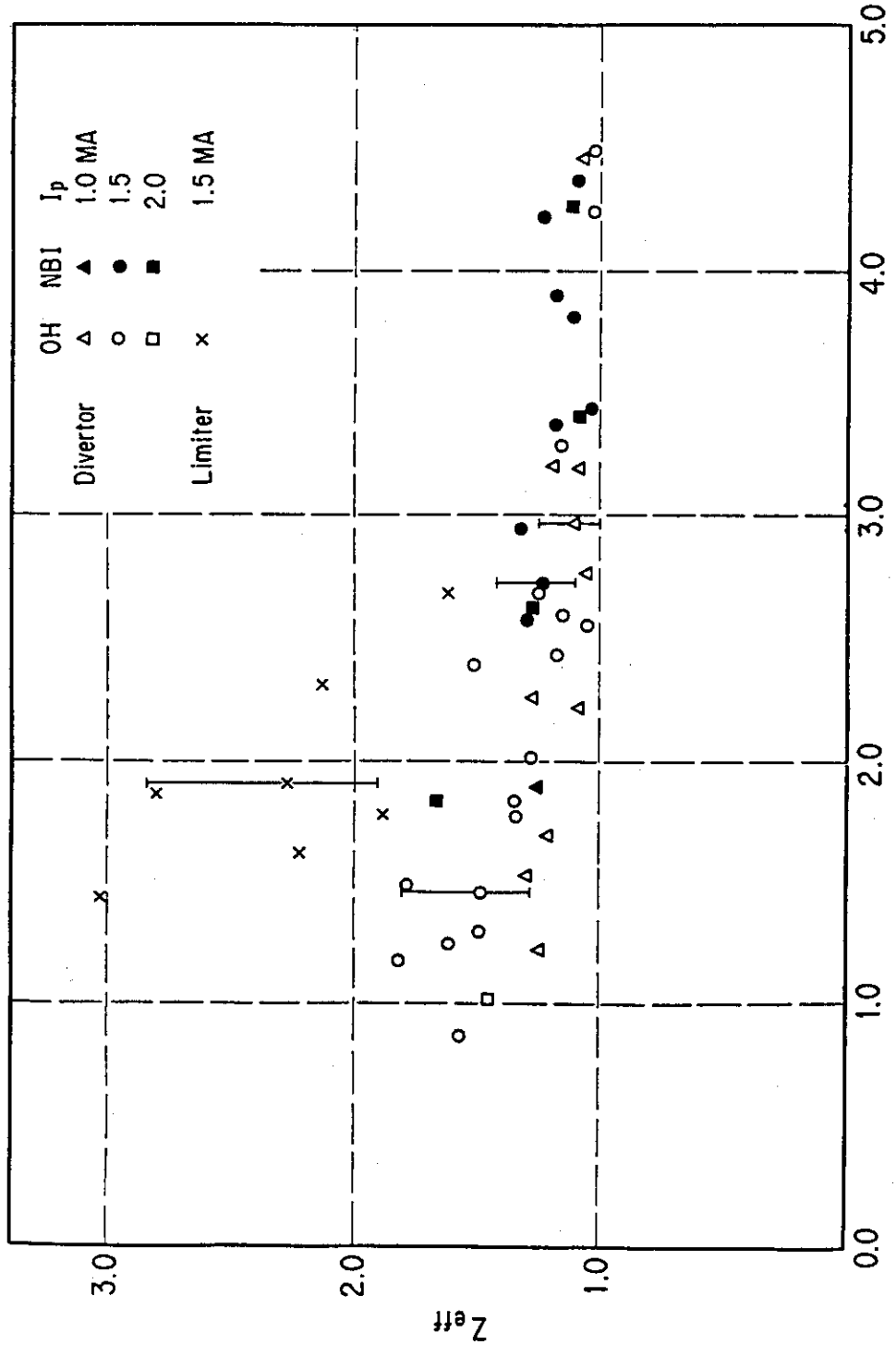

Fig. 9 Effective ionic charge Z_{eff} as a function of electron density

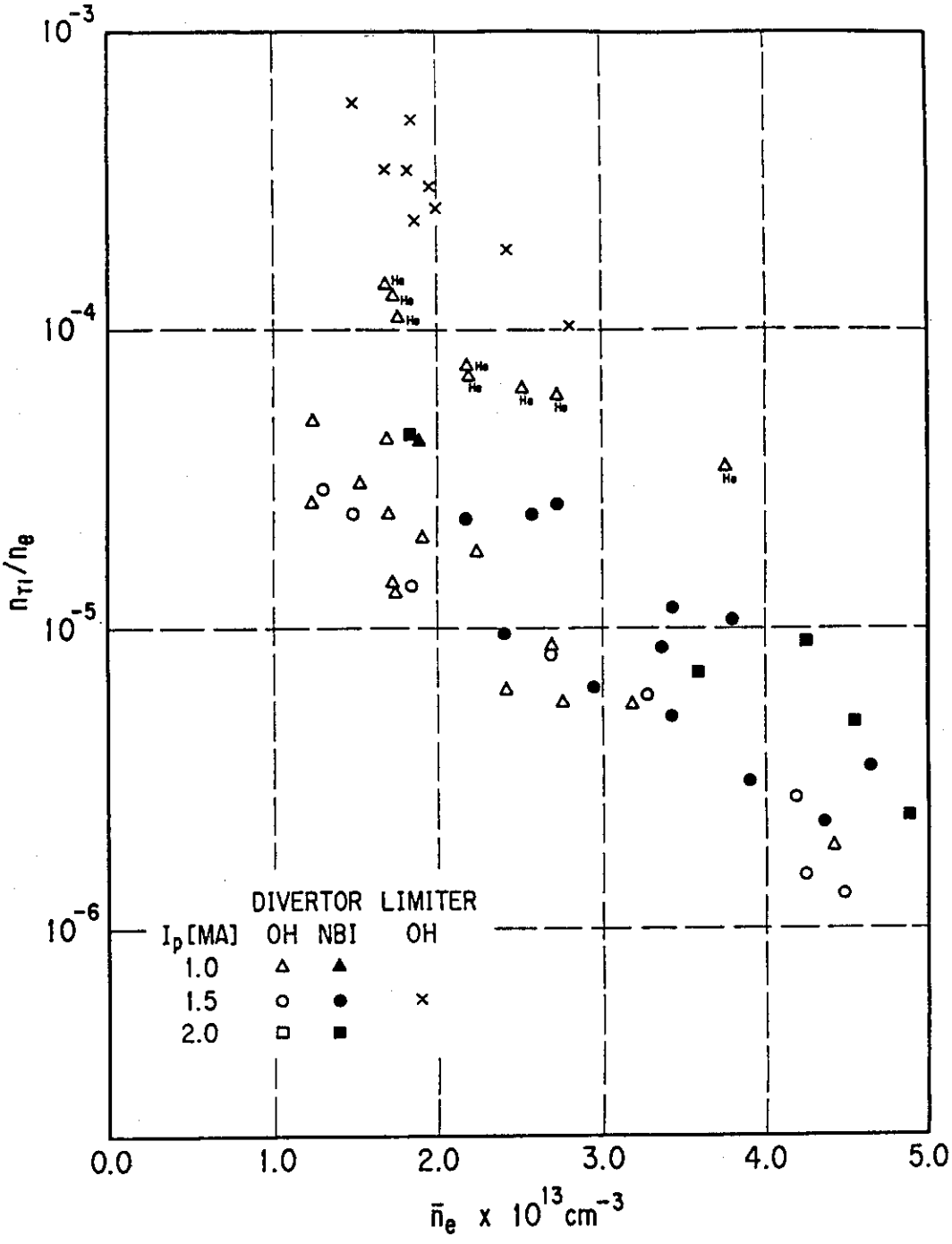

Fig. 10 Titanium concentration as a function of electron density

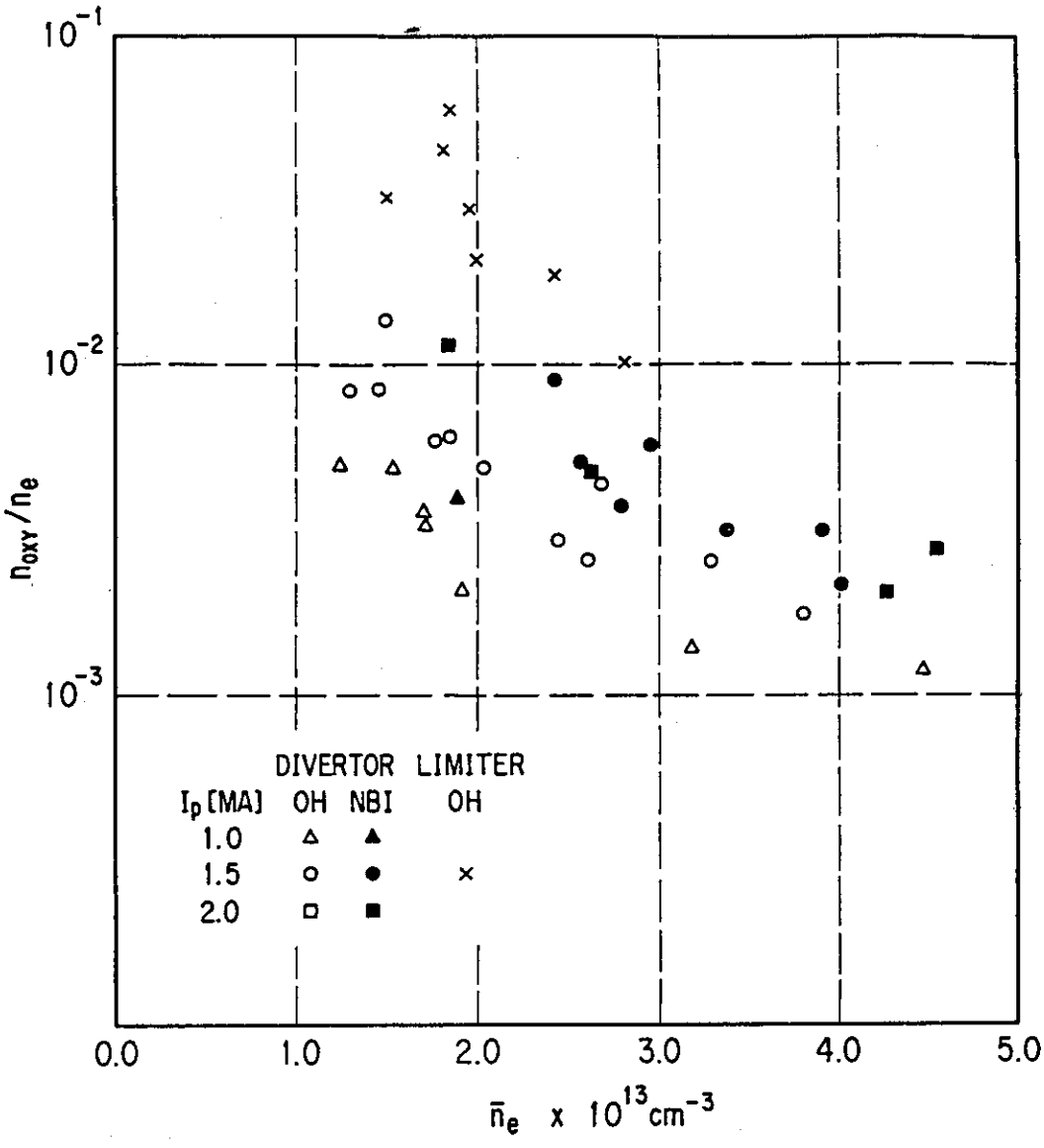

Fig. 11 Oxygen concentration as a function of electron density. Oxygen are considered as the only light impurity.